Chinese Journal of Chemical Engineering 67 (2024) 268–281

Contents lists available at ScienceDirect

Chinese Journal of Chemical Engineering

journal homepage: www.elsevier.com/locate/CJChE

Full Length Article

Growth and inhibition of zinc anode dendrites in Zn-air batteries: Model and experiment

Cuiping He [1, 2], Qingyi Gou [1, 2], Yanqing Hou [1, 2, *], Jianguo Wang [3], Xiang You [5], Ni Yang [1, 4, *], Lin Tian [4], Gang Xie [4], Yuanliang Chen [1, 2]

[1] Kunming University of Science and Technology, State Key Laboratory of Complex Nonferrous Metal Resources Clean Utilization, Kunming 650093, China
[2] Kunming University of Science and Technology, Faculty of Metallurgical and Energy Engineering, Kunming 650093, China
[3] China Copper Co. Ltd, Kunming, Yunnan 650051, China
[4] State Key Laboratory of Advanced Metallurgy for Non-ferrous Metals, Kunming 650051, China
[5] Sichuan Shunying Power Battery Materials Co. Ltd, Sichuan 620076, China

ARTICLE INFO

Article history:
Received 1 July 2023
Received in revised form
19 October 2023
Accepted 15 November 2023
Available online 15 December 2023

Keywords:
Zn-air battery
Zinc anode
Zinc dendrite
Simulated dendrite growth
Inhibit dendrite growth
Phase-field model

ABSTRACT

Zinc (Zn)-air batteries are widely used in secondary battery research owing to their high theoretical energy density, good electrochemical reversibility, stable discharge performance, and low cost of the anode active material Zn. However, the Zn anode also leads to many challenges, including dendrite growth, deformation, and hydrogen precipitation self-corrosion. In this context, Zn dendrite growth has a greater impact on the cycle lives. In this dissertation, a dendrite growth model for a Zn-air battery was established based on electrochemical phase field theory, and the effects of the charging time, anisotropy strength, and electrolyte temperature on the morphology and growth height of Zn dendrites were studied. A series of experiments was designed with different gradient influencing factors in subsequent experiments to verify the theoretical simulations, including elevated electrolyte temperatures, flowing electrolytes, and pulsed charging. The simulation results show that the growth of Zn dendrites is controlled mainly by diffusion and mass transfer processes, whereas the electrolyte temperature, flow rate, and interfacial energy anisotropy intensity are the main factors. The experimental results show that an optimal electrolyte temperature of 343.15 K, an optimal electrolyte flow rate of 40 ml·min^{-1}, and an effective pulse charging mode.

1. Introduction

With the increasing depletion of fossil energy and increasing environmental pressure, countries are desperately looking for clean energy sources to replace fossil energy. Therefore, the development of new clean energy sources is particularly important. Batteries occupy an important position in this field of energy, but traditional batteries are gradually facing elimination, owing to their low safety performance, slow charging speed, environmental pollution, and other shortcomings. Therefore, a new generation of cleaner, more environmentally friendly new energy batteries have been developed, including lithium-air batteries, zinc (Zn)-air batteries, and aluminum-air batteries. Compared with Zn-air batteries, lithium-air batteries have a higher production cost for lithium as the anode active material, and lithium-air batteries also have the problem of lithium dendrite growth; aluminum-air batteries do not have the problem of dendrite growth, but their self-corrosion is more serious during the discharge process. Zn-air batteries have the advantages of a high theoretical energy density (1086 W·h·kg^{-1}), low cost, and lack of environmental pollution [1]. Thus, Zn-air batteries are a strong contender for next-generation energy sources. However, the dendrite growth problem of Zn-air batteries during charge and discharge cycles limits their wide application in transportation and energy storage [2,3]. The dendrite growth of Zn-air batteries can have many adverse effects on the batteries and, in serious cases, can lead to internal short circuits, fire, explosions, and other safety accidents [4]. In addition, as the number of charge/discharge cycles increases, a small number of

* Corresponding authors. Tel.: 86-15987198926 (Y. Hou), Tel.: 15877969695 (N. Yang).
E-mail addresses: hhouyanqing@163.com (Y. Hou), yangnihejiejie@126.com (N. Yang).

https://doi.org/10.1016/j.cjche.2023.11.016
1004-9541/

dendrites may fall off from the Zn electrode during the process, resulting in the formation of "dead dendrites" in the electrolyte and a continuous decay of the battery capacity [5]. Therefore, to improve the cycle life of Zn-air batteries, it is necessary to develop new measures to inhibit the growth of Zn dendrites.

Some researchers have speculated that the changes in the electrode morphology are related mainly to the inhomogeneous distribution of the zincate ions [6] and electrolyte flow [7]. Others have argued that the generation of electrolyte concentration gradients is caused mainly by the inhomogeneous distribution of the current density on the surface of the Zn electrode, in addition to the convection of the electrolyte, which improves the electrolyte concentration gradients [8–11]. Wang *et al.* [12] investigated the effects of trivalent bismuth ions and tetrabutylammonium bromide on dendrite growth in rechargeable Zn-air cells in alkaline zincate solutions. They concluded that Bi^{3+} was preferentially deposited on the Zn electrode side during the polarization of the Zn anode, thereby inhibiting the formation of Zn dendrites. Banik *et al.* [13] showed that the formation of Zn dendrites was inhibited by polyethylene glycol (PEG-200) and that the inhibition became more pronounced with an increasing PEG-200 concentration. Further studies showed that the inhibition of Zn dendrite growth was due mainly to the effect of PEG-200 in weakening the exchange current density during Zn electrodeposition. In addition, the use of pulsed current [14] or enhancing electrolyte convection [15] can increase the ion diffusion rate and reduce the inhomogeneous distribution of the ion concentration at the electrode–electrolyte interface, thereby reducing the ion concentration gradient between the reaction site and native electrolyte and obtaining a uniform electrodeposited Zn morphology. Placing a diaphragm between the cathode and anode slows the growth of Zn dendrites, improving cell life; however, the drawback of this solution is the increased resistance to ion migration [16]. Although solid electrolytes can mitigate dendrite growth, they have poor electrical conductivity and, therefore, increase the voltage difference between charging and discharging [17]. Scanning electron microscopy [18], transmission electron microscopy [19], and atomic force microscopy [20] can be used to analyze the electrode morphologies after experiments but are not suitable for monitoring the dendrite growth process of Zn-air batteries. In contrast, a simulation method can better detect and regulate the entire Zn dendrite growth process and can compensate for the shortcomings of the experimental analysis methods. To gain insight into the physicochemical processes occurring on the surface of Zn electrodes, researchers have developed various models for Zn dendrite growth. Guo *et al.* [21] developed a one-dimensional model for Zn electrodeposition based on diffusion-limited agglomeration and investigated the effects of overpotential on the ion concentration distribution and dendrite growth. However, the microscopic morphology of the dendrites was not represented in the model. Liang *et al.* [22,23] established a model for lithium dendrite growth based on a nonlinear phase-field method and demonstrated that the morphology of the dendrites was consistent with the experimental results. However, this model could only analyze dendrite growth under constant current charging and static electrolyte conditions and did not consider the physicochemical properties of the electrolyte. In addition, morphology control of Zn electrodes can be achieved through the optimal design of the cell structure and magnetic field [24,25], thereby improving the cycle lives of rechargeable Zn-air batteries. Zn-air battery faces many challenges. In addition to dendrite growth, slow oxygen reduction reaction (ORR) kinetics is also a problem that we need to solve. Li *et al.* [26] realized that large-scale production of low-cost bifunctional catalysts is pivotal to promoting the lifetime of Zn-air batteries; hence, they constructed unique bifunctional CoN_3 catalytic sites atomically dispersed on N-doped graphitic carbon nanosheets (CoSA/NCs). Zheng*et al.* [27] reported a cobalt-doped $Mn_2(OH)_3VO_3$ catalyst which serves as ORR and OER active sites, respectively. Cheng *et al.* [28] reported a spherical carbon decorated with FeP and CoP nanoparticles (denoted as FeCoP/NPC) as a bifunctional electrocatalyst which shows prominent activity and reliability for the ORR and OER.

In this study, a two-dimensional phase-field model of dendrite growth in a Zn-air cell was established, and the effects of charging times, different interfacial energy anisotropy strengths, and electrolyte temperatures on the morphology and growth height of Zn dendrites were investigated using this model. We concluded that the growth of Zn dendrites is controlled mainly by diffusion and mass transfer processes. Then, based on the simulated dendrite growth mechanism, experimental schemes were designed for inhibiting Zn dendrite growth, such as raising the electrolyte temperature, increasing the electrolyte flow rate, and using different pulse charging methods.

2. Numerical Simulation

2.1. Geometric model

In this study, a simple two-dimensional geometry was used to simulate the reaction mechanism of the Zn-air battery, as shown in Fig. 1. The simulated domain had a length of 8 mm and a width of 4 mm. To better describe the dynamic changes between the Zn anode and electrolyte interface, an order parameter u was introduced; when $u = 1$, it indicated the Zn anode, when $u = 0$, it indicated the electrolyte, and when $0 < u < 1$, it indicated the liquid-solid phase transition. To avoid the phase transition during the growth of the Zn dendrites being too abrupt, we introduced a step function "Step 1" to describe the changes in the order parameter u, as shown in Fig. 1.

2.2. Phase field model

The basic equations of the phase field include two categories:

One equation, Allen-Cahn, is used to describe the evolution of non-conservative variables (such as phase-field order variables), and its mathematical form is expressed as:

$$\frac{\partial \xi_i}{\partial t} = \nabla \cdot L_i \nabla \frac{\delta F}{\delta \xi_i} \tag{1}$$

Here, ξ_i represents a non-conservative variable, L_i is the interfacial mobility coefficient, F is the total free energy function of the system, and $\delta F/\delta \xi_i$ is variational.

The other equation, Cahn-Hilliard, is used to describe the evolution of conserved variables (such as concentration or potential), and its basic mathematical form is as follows:

$$\frac{\partial c_i}{\partial t} = \nabla \cdot M_i \nabla \frac{\delta F}{\delta c_i} \tag{2}$$

In the above, c_i represents a conserved variable, M_i is interfacial mobility coefficient, and $\delta F/\delta c_i$ is variational.

The establishment of the phase field model is based on the Gibbs free energy of the system. When the temperature is constant, the total Gibbs free energy of zinc dendrites is:

$$G = \int \left[f_{\mathrm{ch}}(u, c) + f_{\mathrm{grad}}(\nabla u) + f_{\mathrm{elec}}(u, c, \varphi) \right] \mathrm{d}V \tag{3}$$

Here, u describes the solid and liquid phases of zinc dendrites, c represents the molar fraction of zinc ions, and φ is the potential.

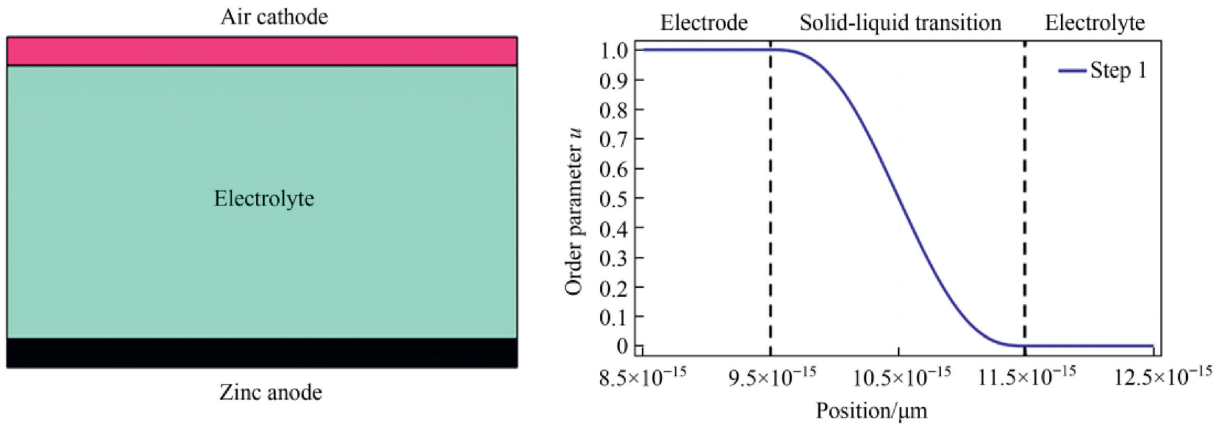

Fig. 1. A schematic diagram of the simulation domain and order parameters.

$f_{ch}(u,c)$ represents the local chemical-free energy density, $f_{grad}(\nabla u)$ represents the gradient energy density at the solid–liquid interface, and $f_{elec}(u,c,\varphi)$ represents the electrochemical energy density.

$$f_{ch}(u,c) = Wu^2(1-u)^2 + c_0RT(c_+ \ln c_+ + c_- \ln c_-) + \sum c_i u_i^{eq} \tag{4}$$

In the above, W is the barrier height, c_+ represents the normalized zinc ion concentration in electrolytes, and c_- normalized anion concentration in the electrolyte. $\sum c_i u_i^{eq}$ represents the free energy density under the standard state, and u_i^{eq} is the equilibrium chemical potential of a substance (such as zinc ions, electronics, or metal atoms).

Anisotropic surface energy is introduced to characterize the roughness of the electrode surface, and the influence of the anisotropy of the free energy of the electrode/electrolyte interface is considered. The interface energy density is expressed by:

$$f_{grad} = \frac{1}{2}\nabla c \cdot k \cdot \nabla c \tag{5}$$

To deeply explore the dendrite growth of Zn-air batteries during charging, we introduce the Ginzburg-Landau and Butler-Volmer equations.

$$j = j^0\left[\exp\left(-\frac{\alpha F\varphi}{RT}\right) - \exp\left(\frac{(1-\alpha)F\varphi}{RT}\right)\right] \tag{6}$$

Eq. (6) is the steady-state electrochemical polarization equation of a single electron electrode reaction. Here, j is the reaction rate of the cathode or anode, and j^0 is the exchange current density of the electrode reaction. α is a symmetry factor, and the charge transfer coefficients of the anode and cathode (α_a and α_c) have a relationship, that is, $\alpha_a = 1-\alpha_c$, $\alpha_c = \alpha$; in this model, $0 < \alpha < 1$. F is the Faraday constant, R is the ideal gas constant, T represents the temperature of the electrolyte, and c_0 represents the initial concentration of the electrolyte. φ represents the overpotential, $\varphi = \Delta\varphi - E^{eq}$, $\Delta\varphi$ is the difference between the positive and negative potentials, and E^{eq} is the standard potential in a half battery.

Below, Eq. (7) is the phase-field equation, and a two-dimensional phase field model for dendrite growth in Zn-air batteries was established based on the Butler-Volmer equations. Eq. (8) is the diffusion equation for the Zn ions, and Eq. (9) is the electric potential equation.

$$\frac{\partial u}{\partial t} = L_\sigma\left[-\frac{\partial}{\partial x}\left(\bar{k}k(\theta)k'(\theta)\frac{\partial u}{\partial y}\right) + \frac{\partial}{\partial y}\left(\bar{k}k(\theta)k'(\theta)\frac{\partial u}{\partial x}\right) + \nabla\cdot\left(\bar{k}k^2(\theta)\nabla u\right) - \frac{\partial g(u)}{u}\right] - L_r\frac{\partial h(u)}{u}\left[\exp\left(-\frac{\alpha nF\varphi}{RT}\right) - \frac{C_{Zn^{2+}}}{c_0}\left(\exp\left(\frac{(1-\alpha)nF\varphi}{RT}\right)\right)\right] \tag{7}$$

In the above, L_σ and L_r represent the interface mobility and reaction rate constant, respectively; $k(\theta) = 1 + \delta\cos(\tau\theta)$ represents the interfacial energy anisotropy, δ is the anisotropy strength, and τ is the anisotropy mode number. $\bar{k}$ is the gradient energy polynomial coefficient, and $g(u) = Wu^2(1-u)^2$ is a double-well free energy function for describing the two equilibrium states of the electrode ($u = 1$) and the electrolyte ($u = 0$). $h(u) = u^3(6u^2-15u+10)$ is the interpolation function of the electrode-electrolyte interface. n represents the valence of the Zn ions. α, F, φ, R, and T have the same value as in Eq. (6).

$$\frac{\partial C_{Zn^{2+}}}{\partial t} = \nabla\cdot\left(D_{Zn^{2+}}(u)\nabla u\right) + \frac{D_{Zn^{2+}}(u)C_{Zn^{2+}}F}{RT}\nabla\varphi - \lambda c_s\frac{\partial u}{\partial t} \tag{8}$$

Here, $D_{Zn^{2+}}(u) = D^e h(u) + D^s(1-h(u))$ describes the diffusion of the Zn ions in the electrode and electrolyte, and D^e and D^s represent the effective diffusion coefficients of the Zn ions in the electrode and electrolyte, respectively. λ is a constant, and c_s represents the positional density of Zn, *i.e.* the reciprocal of the volume of 1 mole of Zn atoms, that is, $c_s = 1/V_{Zn} = m_{Zn}/\rho_{Zn} = 1.09\times10^5$ mol·m^{-3}. m_{Zn} and ρ_{Zn} represent the molar mass and density of Zn, respectively.

$$\frac{\partial\varphi}{\partial t} = \nabla\cdot\left(\sigma_{Zn^{2+}}(u)\nabla\varphi\right) - nFc_s\frac{\partial u}{\partial t} \tag{9}$$

In the above, $\sigma_{Zn^{2+}} = \sigma^e h(u) + \sigma^s(1-h(u))$ describes the conductivity of the electrode and electrolyte, and σ^e and σ^s represent the electrode and electrolyte conductivities, respectively.

The General Form partial differential equation in COMSOL is used to establish the control equation for dendrite growth. The General Form of PDE is shown in Eq. (4).

$$e_a\frac{\partial^2 u}{\partial t^2} + d_a\frac{\partial u}{\partial t} + \nabla\cdot\Gamma = f \tag{10}$$

Table 1
Phase field modeling parameters

Parameter	Symbol	Value
Interfacial mobility	L_σ	$1 \times 10^{-6}\ m^3 \cdot (J \cdot s)^{-1}$
Reaction constant	L_r	$0.5 s^{-1}$
Gradient energy coefficient	$\bar{k}$	$1 \times 10^{-10}\ J \cdot m^{-1}$
Barrier height	W	$3.5 \times 10^5\ J \cdot m^{-3}$
Modulus of anisotropy	τ	4
Diffusion coefficient in electrode	D^e	$2 \times 10^{-15}\ m^2 \cdot s^{-1}$
Diffusion coefficient in solution	D^s	$2 \times 10^{-15}\ m^2 \cdot s^{-1}$
Conductivity in electrode	σ^e	$1 \times 10^7\ S \cdot m^{-1}$
Conductivity in solution	σ^s	$0.1\ S \cdot m^{-1}$
Valency of Zn ion	n	2
Faraday constant	F	$9.65 \times 10^4\ C \cdot mol^{-1}$
Molar gas constant	R	$8.314\ J \cdot (mol \cdot K)^{-1}$

Here, e_a represents the mass factor, d_a represents the damped mass factor, Γ represents the conserved flux, and f represents the source term.

Above all phase field parameters mentioned are shown in Table 1.

To couple the phase field Eq. (1) with the partial differential Eq. (4), it is necessary to transform Eq. (1) into the form of Eq. (4), and the results are as follows.

$$e_{a1} = 0$$

$$d_{a1} = 1$$

$$\Gamma_1 = \begin{vmatrix} L_\sigma \cdot \bar{k} k(\theta) k'(\theta) \dfrac{\partial u}{\partial y} - \bar{k} k^2(\theta) \dfrac{\partial u}{\partial x} \\ -L_\sigma \cdot \bar{k} k(\theta) k'(\theta) \dfrac{\partial u}{\partial x} - \bar{k} k^2(\theta) \dfrac{\partial u}{\partial y} \end{vmatrix}$$

$$f_1 = -L_\sigma \cdot \frac{\partial g(u)}{u} - L_r \frac{\partial h(u)}{u} \left[\exp\left(-\frac{\alpha n F \varphi}{RT} \right) - \frac{C_{Zn^{2+}}}{C_0} \left(\exp\left(\frac{(1-\alpha) n F \varphi}{RT} \right) \right) \right]$$

By coupling Eq. (2) with Eq. (4), the following results can be deduced.

$$e_{a2} = 0$$

$$d_{a2} = 1$$

$$\Gamma_2 = \begin{vmatrix} -D_{Zn^{2+}}(u) \left(\dfrac{\partial C_{Zn^{2+}}}{\partial x} + \dfrac{C_{Zn^{2+}} F}{RT} \dfrac{\partial \varphi}{\partial x} \right) \\ -D_{Zn^{2+}}(u) \left(\dfrac{\partial C_{Zn^{2+}}}{\partial y} + \dfrac{C_{Zn^{2+}} F}{RT} \dfrac{\partial \varphi}{\partial y} \right) \end{vmatrix}$$

$$f_2 = -\lambda c_s \frac{\partial u}{\partial t}$$

The same can be obtained, and the following results can be deduced by coupling Eq. (3) with Eq. (4).

$$e_{a3} = 0$$

$$d_{a3} = 1$$

$$\Gamma_3 = \begin{vmatrix} -\sigma_{Zn^{2+}}(u) \dfrac{\partial \varphi}{\partial x} \\ -\sigma_{Zn^{2+}}(u) \dfrac{\partial \varphi}{\partial y} \end{vmatrix}$$

$$f_3 = -nFc_s \frac{\partial u}{\partial t}$$

2.3. Simulation method

We apply the finite element numerical analysis method to establish the model. The main steps of COMSOL Multiphysics 6.0 finite element analysis include the following: select the physical field, establish the model, select parameters, calculate the simulation, and use the result in analysis. In the selection of physical fields, COMSOL Multiphysics 6.0 can choose the required physical fields according to their requirements and directly combine these physical fields for full coupling. The equation for deposited zinc is $Zn^{2+} + 2e^- = Zn$. The two-dimensional model was set as an 8 μm × 4 μm rectangle. The upper boundary of the rectangle represents the air cathode, and the lower boundary of the rectangle represents the zinc anode. The values of the input parameters are obtained from the references or the material properties that come with COMSOL Multiphysics 6.0. The detailed parameter values are shown in Table 1. The writing of general partial differential equations is the most momentous. The phase field equation, zinc ion concentration equation, and electric potential equation are transformed into general partial differential equations, and the conserved flux, primary phase, damping coefficient, and mass coefficient are written into the equations.

Finally, the rationality of the mesh division is crucial for the accuracy and convergence of the simulation results. When the mesh division is too coarse, the deviation between the calculated result and the accurate value is large. Therefore, the finer the mesh division is, the more accurate the results. However, when the mesh is excessively dense, it will lead to an increased amount of computation. Therefore, a reasonable mesh division is required for different models. In this model, a free quadrilateral mesh was used with a maximum element size of 0.05 μm, a minimum element size of 0.005 μm, a maximum element growth rate of 1.3, and a curvature factor of 0.3. At this point, we can directly calculate the simulation results.

3. Experiments

To further verify the reliability of the proposed model and obtain an efficient way to inhibit dendritic growth in zinc-air batteries, an experimental study was conducted. A Zn electrode with a length of 3 cm, a width of 2 cm, and a thickness of 0.2 cm was manufactured. The Zn electrode was perforated and connected to a copper wire and then sealed with an epoxy resin adhesive and epoxy resin curing agent while reserving 2 cm^2 of the surface as the working electrode. The working electrode was polished, initially by polishing from coarse to fine sandpaper step-by-step and then by polishing with alumina polishing powder until there were no scratches on the surface of the electrode. Then, the residual polishing powder on the surface of the electrode was washed away with distilled water, and the electrode was placed for use. A schematic diagram of the Zn anode is shown in Fig. 2. The cathode material was a bifunctional electrode material, with an air-negative layer on one side and a catalytic layer with cobalt oxide attached on the other sides; and the distance between the anode and cathode

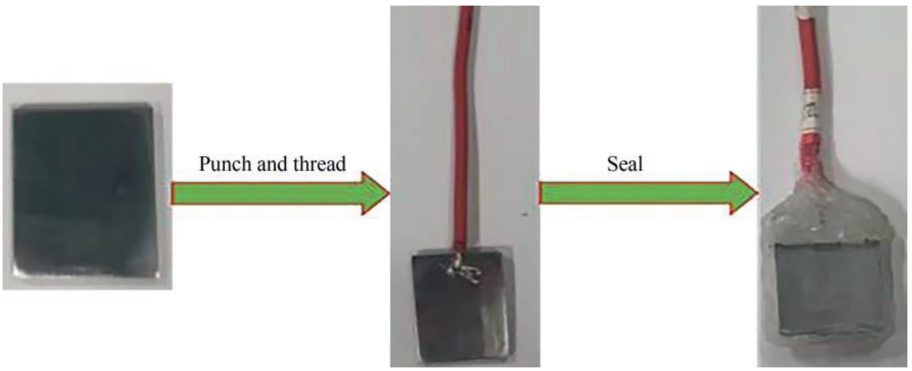

Fig. 2. A schematic diagram of the preparation of the Zn anode.

was 5 mm. The air cathode in the experiments is a commercial air electrode consisting of carbon, cobalt oxide catalyst, polyfluorotetraethylene binder, and nickel foam. The size of the air electrode is 7 cm × 6 cm, as shown in Fig. 3. Fig. 3(a) shows the air-enriched layer; Fig. 3(b) shows the catalytic oxide layer.

The experiments were sequentially carried out by alloying the Zn anode, transforming it with different pulses, altering the electrolyte flow rate, and changing the electrolyte temperature. In these experiments, changing pulses, electrolyte flow rate, and electrolyte temperature were carried out using the device shown in Fig. 4. Fig. 4(a) shows a Zn-air battery, and the 7 mol·L^{-1} KOH electrolyte with saturated ZnO was injected into the Zn-air battery box. The device in Fig. 4(a) can be connected to the blue battery test system to change the pulses. The electrolyte flow rate can be changed when the device is connected to a peristaltic pump. The completed experimental setup is shown in Fig. 5(b).

The intermediate frequency induction melting furnace and the casting plate mold were preheated, when the alloying experiment was carried out. Then, pure zinc (purity 99.995% or more) with other metals that needed to be mixed was put into the intermediate frequency induction melting furnace until the pure Zn and added metal were completely melted, and then, the floating slag on the

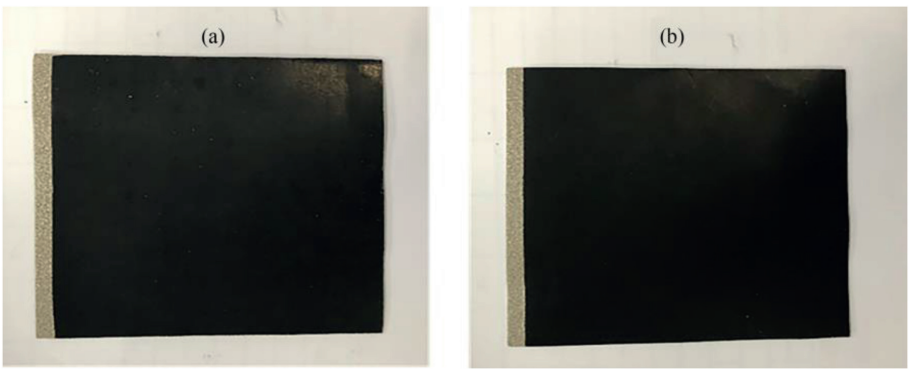

Fig. 3. Air electrode: (a) air enrichment layer; (b) catalyst layer.

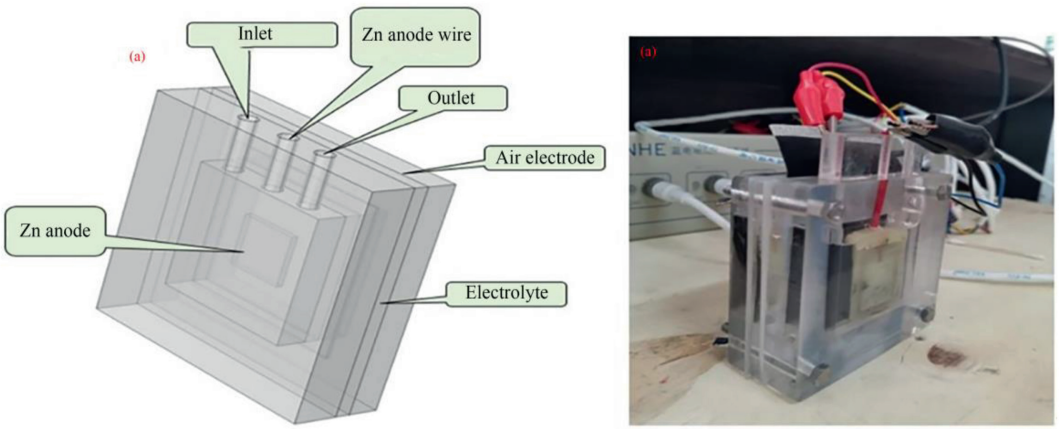

Fig. 4. Experimental device diagram (a) zinc-air battery box; (b) zinc-air battery experimental connection diagram.

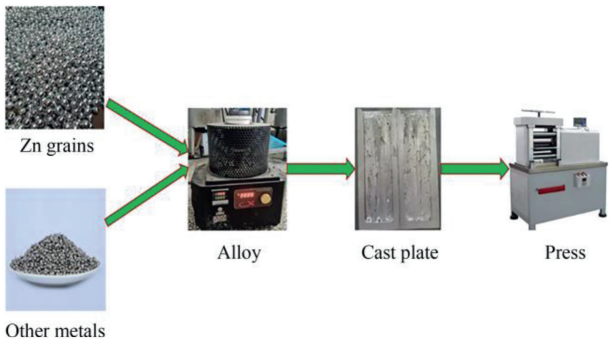

Fig. 5. Alloying process of the zinc anode.

surface was completely salvaged. After warming for 10 min, the molten metal was poured into the cast plate mold, and then the surface temperature of the mold was cooled to room temperature before opening the mold, and sending the metal plate to the forging machine for pressing. The thickness of the plate was reduced by 1 mm in turn during the pressing process, pressing finished when the thickness of the plate was 2 mm. The metal plate was finally made into a Zn anode with a 2 cm width and 3 cm length.

4. Results and Discussion

The dendrite growth mechanism of Zn-air batteries was verified, and we concluded that the growth of Zn dendrites is controlled mainly by diffusion and mass transfer processes first. The Zn ion concentration gradient and potential gradient are the main driving forces for Zn dendrite growth, while the interfacial anisotropy strength, electrolyte temperature, and electrolyte flow rate are the main influencing factors for Zn ion diffusion and mass transfer processes. In addition, these methods can also inhibit the growth of dendrites, such as the alloying of Zn anodes and the adoption of different pulses. These factors on the dendrite growth of Zn-air batteries have been discussed through simulations and experiments.

4.1. Model verification

Fig. 6 shows the evolution of the phase-field sequence parameters u, Zn ion concentration distribution, and potential distribution with the charging time, as obtained by solving Eqs. (1)–(3). As shown in Fig. 6(a), the growth height of the dendrites in the Zn-air battery gradually increases with time during the charging process. As shown in Fig. 6(b), the distribution of the Zn ions is not uniform within a certain range on the surface of the Zn dendrite, and the concentration gradient region expands as the charging time increases from 1 to 25 s. In addition, it is evident from the enlarged view of the dendrite tip shown in Fig. 6(b) that as the Zn dendrite grows, additional Zn ions migrate toward the tip of the dendrite, resulting in the preferential deposition of additional Zn ions at this location and increasing the dendrite height. As shown in Fig. 6(c), with the continuous growth of Zn dendrites, the potential distribution in the electrolyte becomes increasingly uneven (especially at the tip of the dendrite, where the potential gradient is the largest), resulting in an excessive local current density at the tip of the dendrite. Thus, most Zn is deposited at the tip during each deposition process. Fig. 7 shows the length of the largest Zn dendrite during the charging process of the Zn-air battery. It is apparent from Fig. 7 clearly shows that the growth height of the dendrite backbone gradually increases from 0.001 μm to 4 μm and that the dendrite height increases with increasing charging time. From the above analysis, we can conclude that dendrite growth gradually increases with the charging time; moreover, the growth height increases. The ion concentration gradient and the potential gradient are the two main driving forces for the Zn dendrite growth.

To verify the reliability of the proposed phase field model, constant-current charging experiments of Zn-air batteries were carried out with a charging current density of 90 $mA \cdot cm^{-2}$. Fig. 8 shows the dendrite growth morphology of Zn-air batteries with charging time, and Fig. 8(a)–(d) shows that the longer the constant-current charging time is, the higher the growth height of Zn dendrites. The experimental results are consistent with the evolution of dendrite growth with time in Fig. 7. Therefore, the proposed phase field model has some reference value to study the challenges faced by Zn-air batteries.

4.2. Numerical results

4.2.1. Effect of energy anisotropy strength on dendritic growth

Fig. 9(a)–(d) shows the relationship between the evolutionary morphology of the dendrite growth and the intensity of the interfacial energy anisotropy. When $\delta = 0.00$, the side branches of the dendrite backbone grow longer, and there are fewer nucleation sites on the Zn electrode. When $\delta = 0.01$ and $\delta = 0.07$, Fig. 9 shows that the growth height of the dendrites increases with increasing interfacial energy anisotropy intensity. The number of nucleation sites on the side of the Zn electrode also increases, and additional dwarf Zn dendrites are grown. From Fig. 9(d) and Fig. 10, when $\delta = 0.1$, the growth height of the Zn dendrite decreases, mainly because with the increase in the anisotropic strength of the interface energy, the trunk of the dendrite diverges; simultaneously, the tip radius of the dendrite decreases, making the dendrite sharper and increasing the risk of the dendrite piercing the diaphragm. Therefore, with the increase in anisotropic strength, the nucleation site and dendrite growth rate also increase. Simultaneously, the number of lateral branches decreases sharply, and the tips of the dendrites become sharper and sharper. The greater the strength of the anisotropy is, the greater the energy of the interface anisotropy. Larger interfacial energy can drive the rapid growth of dendrites, particularly the dendrite tips, due to the large concentration gradient of Zn ions at the dendrite tip. These can accelerate the deposition of Zn ions, thereby promoting the rapid growth of the dendrite tip.

4.2.2. Effect of electrolyte temperature on dendritic growth

The deposition of Zn ions on the side of the Zn electrode is closely related to the diffusion of the ions in the electrolyte. With the continuous deposition of Zn ions, the concentration of Zn ions near the tip of the Zn dendrite decreases, thereby increasing the gradient of the ion concentration at the tip of the dendrite and resulting in the preferential deposition of Zn ions at the tip every time it is charged. Increasing the temperature of the solution can strengthen the Brownian motion of the ions in the solution and enhance their diffusion. As shown in Fig. 11(a)–(h), the lower the electrolyte temperature is, the higher the growth of Zn dendrites. With an increase in the electrolyte temperature, the dendrite growth height is significantly inhibited. When the electrolyte temperature is 343.15 K, the inhibition effect on the Zn dendrites is optimal. From Fig. 12, the growth height of the Zn dendrite can be seen to decrease with increasing electrolyte temperature, and the growth height of the Zn dendrite is 3.465 μm when the electrolyte temperature is 278.15 K. When the electrolyte temperature increases to 343.15 K, the growth height of the Zn dendrite decreases to 1.420 μm, and the inhibition efficiency of the Zn dendrite reaches as high as 59%. Therefore, we conclude from the simulation results

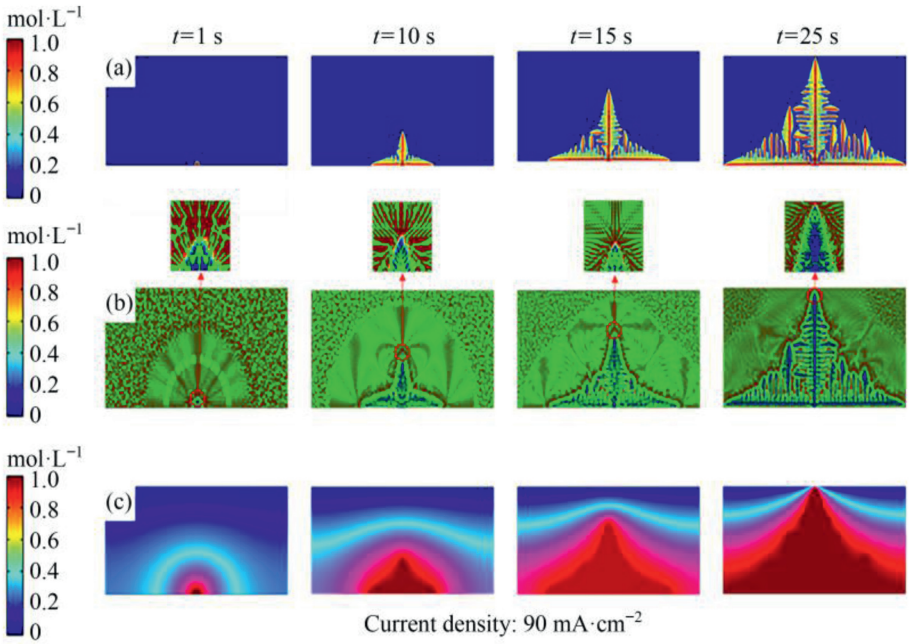

Fig. 6. Evolution diagram of dendrite growth with time, (a) change in the phase sequence parameter μ, (b) zinc ion concentration distribution, (c) potential distribution.

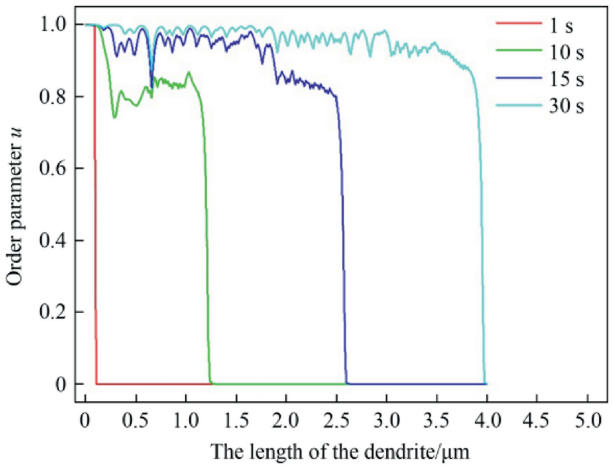

Fig. 7. Maximum length diagram of dendrite growth.

that increasing the electrolyte temperature can inhibit the growth of dendrites, particularly when the electrolyte temperature is 343.15 K. As noted above, the best inhibition effect is achieved at an electrolyte temperature of 343.15 K.

4.3. Experimental results

4.3.1. Dendrite suppression by surface alloying of the zinc anode

The numbers of anisotropic strength for pure zinc, Zn-2.5% In alloy, and Zn-3.5% In alloy are 0, 0.07, and 0.1, respectively. The growth of zinc dendrites can be inhibited more effectively with increasing anisotropic strength as shown in Fig. 9. Therefore, zinc alloying experiments can be conducted to explore the effect of zinc-based alloys on dendrites. Experimental results show that anisotropic strength of zinc anodes can be changed by zinc base alloys. The height of dendrite growth can be suppressed effectively by zinc alloying, the anisotropic strength of which can be changed with alloying zinc by adding different content In.

Experiments were carried out with different contents of Zn-In alloy for the first step. In was added to the anode to form Zn-In alloy, and then constant-current charging was conducted. Fig. 13 (a) shows the surface morphology of the pure Zn anode, and Fig. 13(d) shows the surface morphology when 3.5% In was added to the pure zinc anode. Clearly, the surface of the Zn anode becomes smoother when 3.5% In is added, and the defects are reduced on the interface of the alloyed Zn anode. In addition, the surface of the Zn anode is refined after alloying, and the refined grains can reduce the anisotropic strength of the interfacial energy. The number of Zn dendrites and the growth height gradually decreases with increasing In, as shown in Fig. 13(b), (c), (e), and (f). The experimental results show that the inhibition effect of Zn dendrites is optimal when the proportion of In is 3.5%. Therefore, it is effective to add In into pure Zn to inhibit dendrite growth.

Experiments were carried out on the inhibition of Zn dendrites by different contents of Zn-Yb alloys. The alloys would form a eutectic to refine the grains of the Zn anode when Zn and Yb formed an alloy, making the surface of the Zn anode smoother and reducing the diffusion resistance of ions on the surface of the Zn anode. Fig. 14(a)–(d) show that the grains become finer on the surface of the Zn anode when Yb is added to pure Zn. The inhibition force on the growth of Zn dendrites increases with the increasing proportion of Yb in the Zn anode, as shown in Fig. 14(b), (c), (e), and (f). The networked dendrites slowly transform into rounded dendrites from Fig. 14(c) to (f). The Zn—Yb alloy not only refines grains but also has weak magnetic properties which have an adsorption capability for the Zn dendrites, resulting in the deposition of Zn dendrites. However, the cost of the Zn-air battery is considered because of the expensive Yb. Yb will not add to pure Zn when the content of Yb reaches 6.5%. In all experiments, the inhibition effect on the growth of Zn dendrites will also be optimal when the proportion of Yb is 6.5%.

4.3.2. Dendrite suppression by charge circuit of electrical impulses

As shown in Fig. 15, different pulse charging methods are effective in inhibiting the growth of Zn dendrites. Fig. 15(a) shows that the growth of Zn dendrites is very vigorous when

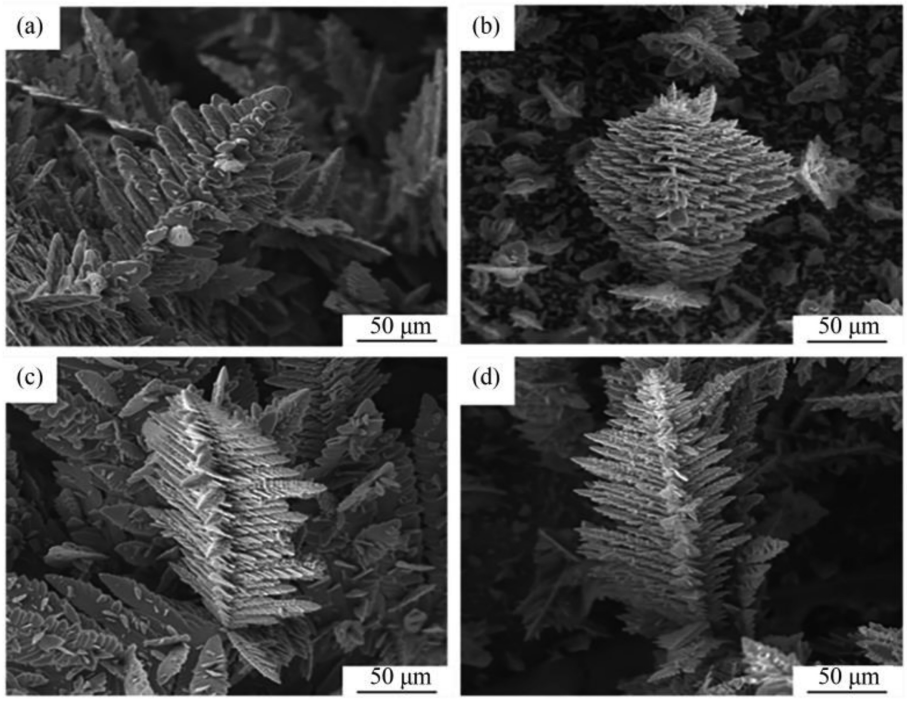

Fig. 8. Change in zinc dendrite growth with time (a) the constant current charge for 5 min. (b) The constant current charge for 8 min. (c) The constant current charge for 15 min. (d) The constant current charge for 20 min.

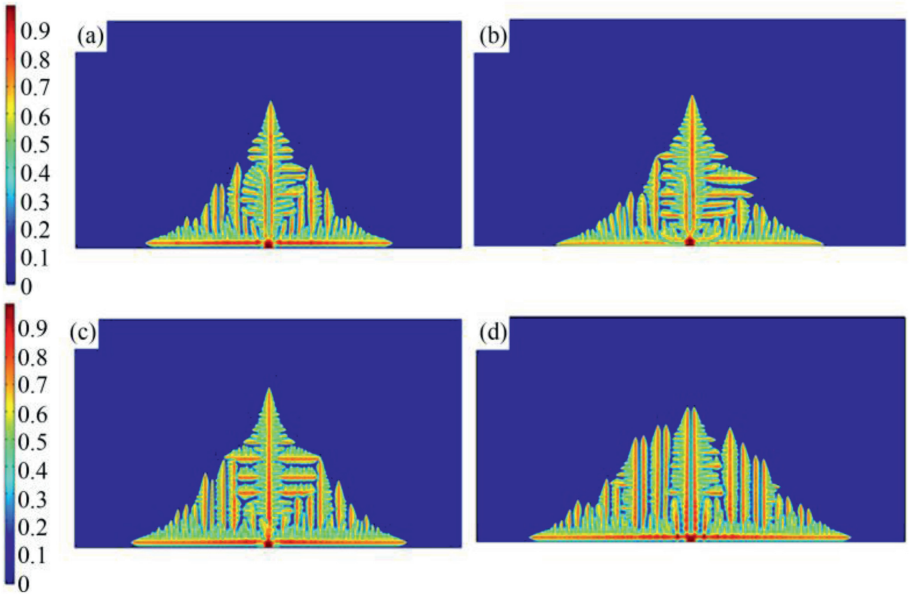

Fig. 9. Simulation diagram of dendrite growth and evolution under different anisotropic intensities: (a) $\delta = 0.00$, (b) $\delta = 0.01$, (c) $\delta = 0.07$, and (d) $\delta = 0.1$.

using the traditional charging method. As shown in Fig. 16(b)–(e), when the Zn-air battery is charged, not only is the number of Zn dendrites reduced but also the heights and shapes of Zn dendrites are greatly changed (from tall dendrites to short shrubs, and finally to granular bulges), mainly because the pulse charging mode of the forward pulse and reverse pulses significantly weakens the potential gradient at the tip of the Zn dendrite, making the local current density uniform. Thus the Zn ions will have additional opportunities to deposit on the concave side of the Zn electrode, thereby inhibiting the growth of Zn dendrites. In particular, the pulse charging method of standing for 5 s, a forward pulse for 10 s, standing for 5 s, and a reverse pulse for 10 s, as shown in Fig. 15(e), is the best way to inhibit dendritic growth in the Zn-air battery.

4.3.3. Effect of electrolyte temperature on dendrite suppression

The effect of temperature on dendritic growth has been investigated by experiments and simulations. The diffusion rate of zinc atoms is slower in lower temperature, which increases the concentration polarization of zinc ion. Thus, the overpotential enlarges,

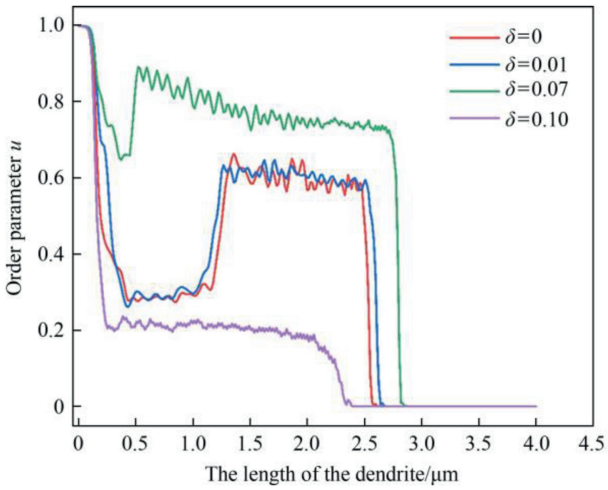

Fig. 10. Maximum length of dendrite growth under different anisotropic strengths.

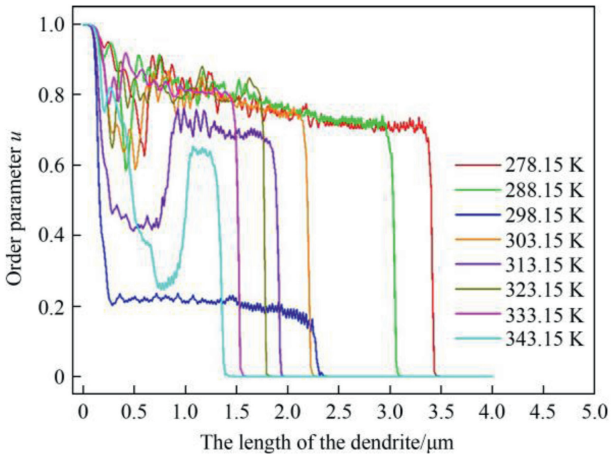

Fig. 12. Maximum length of dendrite growth at different temperatures.

based on which the growth height can be accelerated in lower temperature. Therefore, it is beneficial for promoting liquid phase mass transfer and inhibiting the growth of dendrites appropriately increasing the system temperature within a certain temperature range. The service life of zinc air batteries can be affected by dendrite growth, side reaction, and hydrogen evolution corrosion, in which he occurrence of hydrogen evolution corrosion is greater than 400 °C [29]. Therefore, the optimal temperature (343.15 K) is feasible for inhibiting dendrite growth in this study.

The effect of the electrolyte temperature on Zn dendrite growth in Fig. 16 shows that the growth height of Zn dendrites is significantly suppressed as the electrolyte temperature increases. When the electrolyte temperature was in the range of 298.15 K–313.15 K, the inhibition of the growth height of the Zn dendrites was less explicit, but when the electrolyte temperature was in the range of 343.15 K, the temperature not only effectively inhibited the growth of Zn dendrites but also evidently changed their morphology. The morphology of the Zn dendrites changed from dendritic to leafy dendrites and finally to dwarf stone-like crystals, mainly because increasing the electrolyte temperature facilitates the diffusion of Zn ions in the electrolyte, effectively reducing the Zn ion concentration gradient at the tip of zinc dendrites, providing the opportunity to deposit Zn ions at other locations on the Zn electrode interface, thus inhibiting the growth of Zn dendrites. In summary, we conclude that the optimal electrolyte temperature for inhibiting Zn dendrite growth is 343.15 K.

4.3.4. Effect of electrolyte flow rate on dendrite suppression

As shown in Fig. 17(a), when the electrolyte of the Zn-air cell is static, the Zn dendrite grows upright, and as the flow rate of the electrolyte increases from 10 ml·min^{-1} to 40 ml·min^{-1}, the growth direction of the Zn dendrite gradually changes. The growth direction of the Zn dendrite gradually changes from upright growth to spiral growth, as shown in Fig. 17(e), and finally changes to creeping growth close to the side of the Zn electrode, as shown in Fig. 17(f), mainly because the electrolyte flow accelerates the mass transfer process of the Zn ions in the

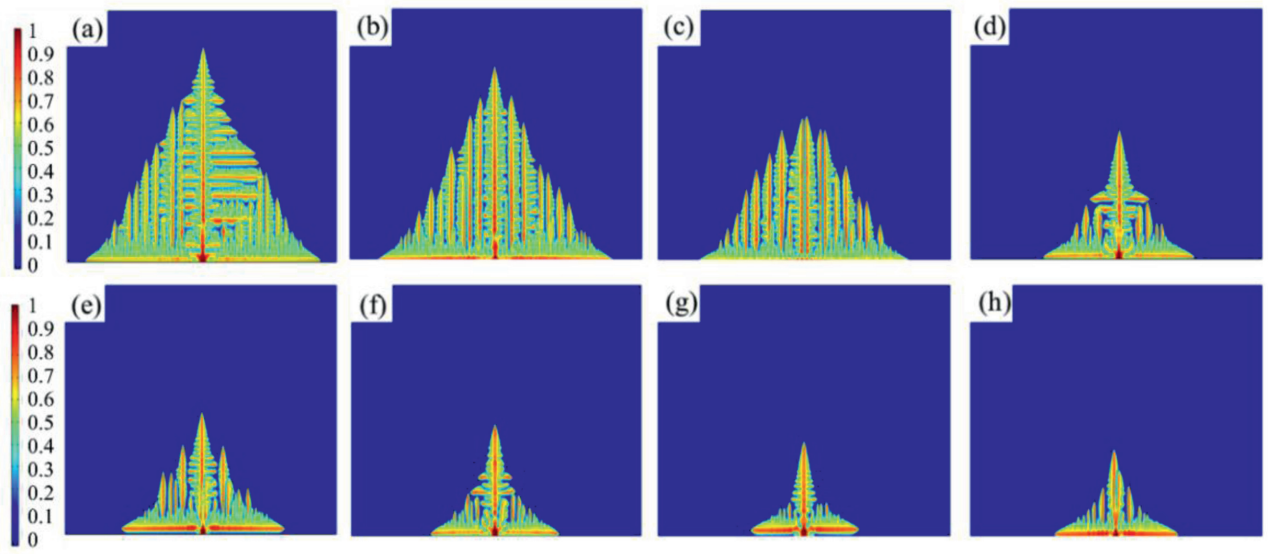

Fig. 11. Simulation diagram of zinc dendrite growth with electrolyte temperature, where respectively indicate that the temperature of the electrolyte is 278.15 K (a), 288.15 K (b), 298.15 K (c), 303.15 K (d), 313.15 K (e), 323.15 K (f), 333.15 K (g), and 343.15 K (h).

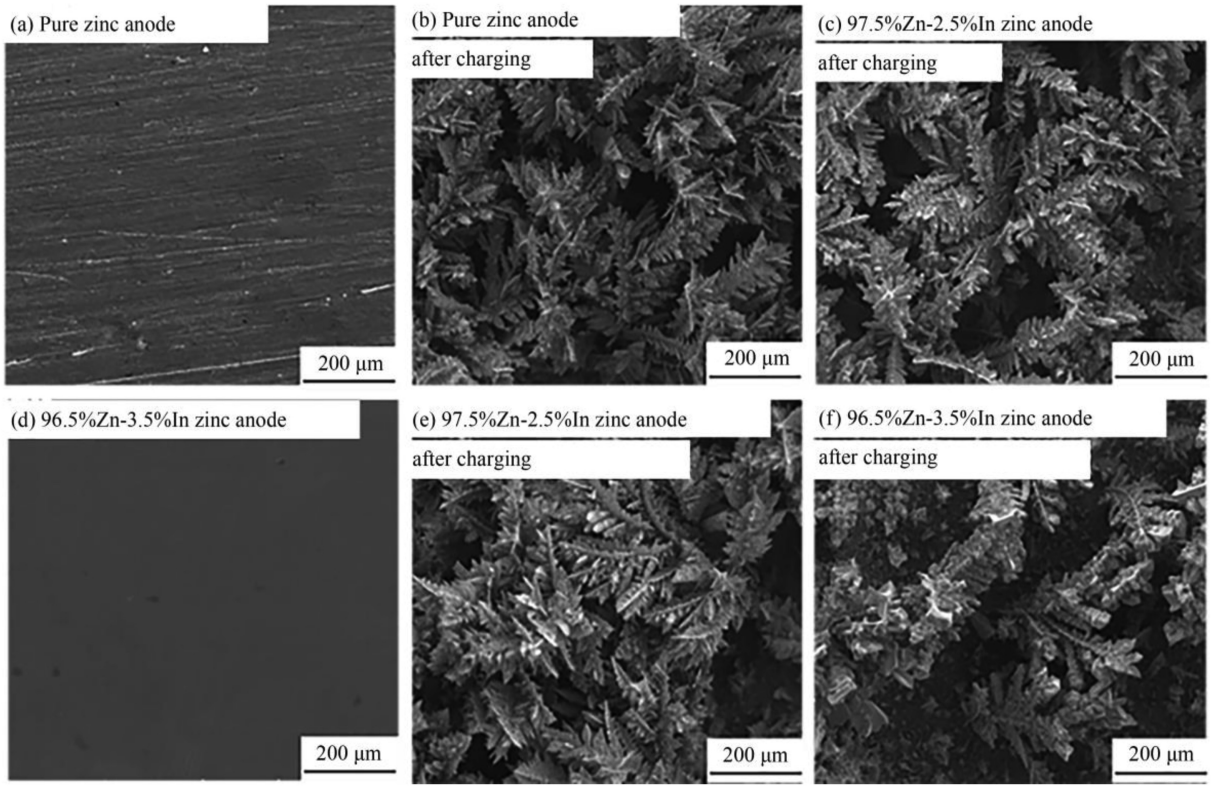

Fig. 13. Inhibition effect of different Zn-In alloys on zinc dendrite growth, (a) pure zinc anode before constant current charging; (b) pure zinc anode after constant current charge; (c) 487.5 g Zn-12.5 g In of zinc anode after constant current charge; (d) 482.5 g Zn-17.5 g In of zinc anode before constant current charging; (e) 487.5 g Zn-12.5 g In of zinc anode after constant current charge; (f) 482.5 g Zn-17.5 g In of zinc anode after constant current charge.

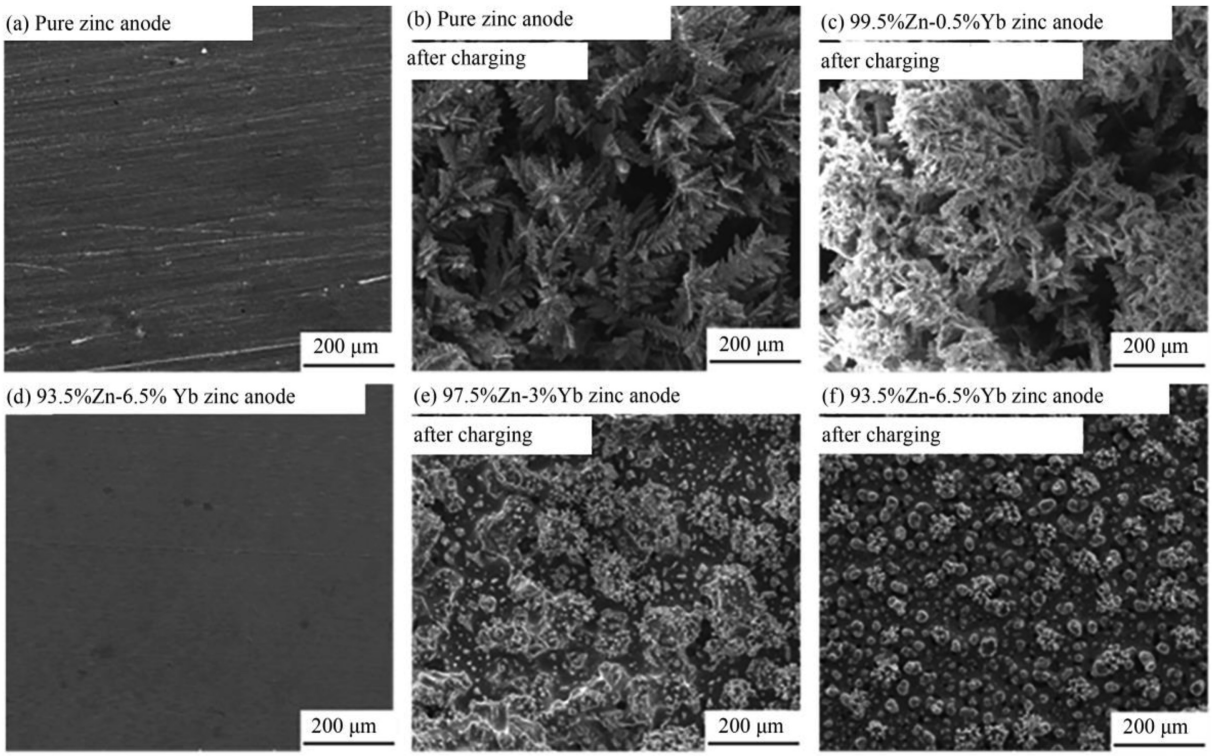

Fig. 14. Inhibition effect of different Zn-Yb alloys on zinc dendrite growth, (a) pure zinc anode before constant current charge; (b) pure zinc anode after constant current charge; (c) 497.5 g Zn-2.5 g Yb of zinc anode after constant current charge; (d) 467.5 g Zn-32.5 g Yb of zinc anode before constant current charge; (e) 485 g Zn-15 g Yb of zinc anode after constant current charge; (f) 467.5 g Zn-32.5 g Yb of zinc anode after constant current charge.

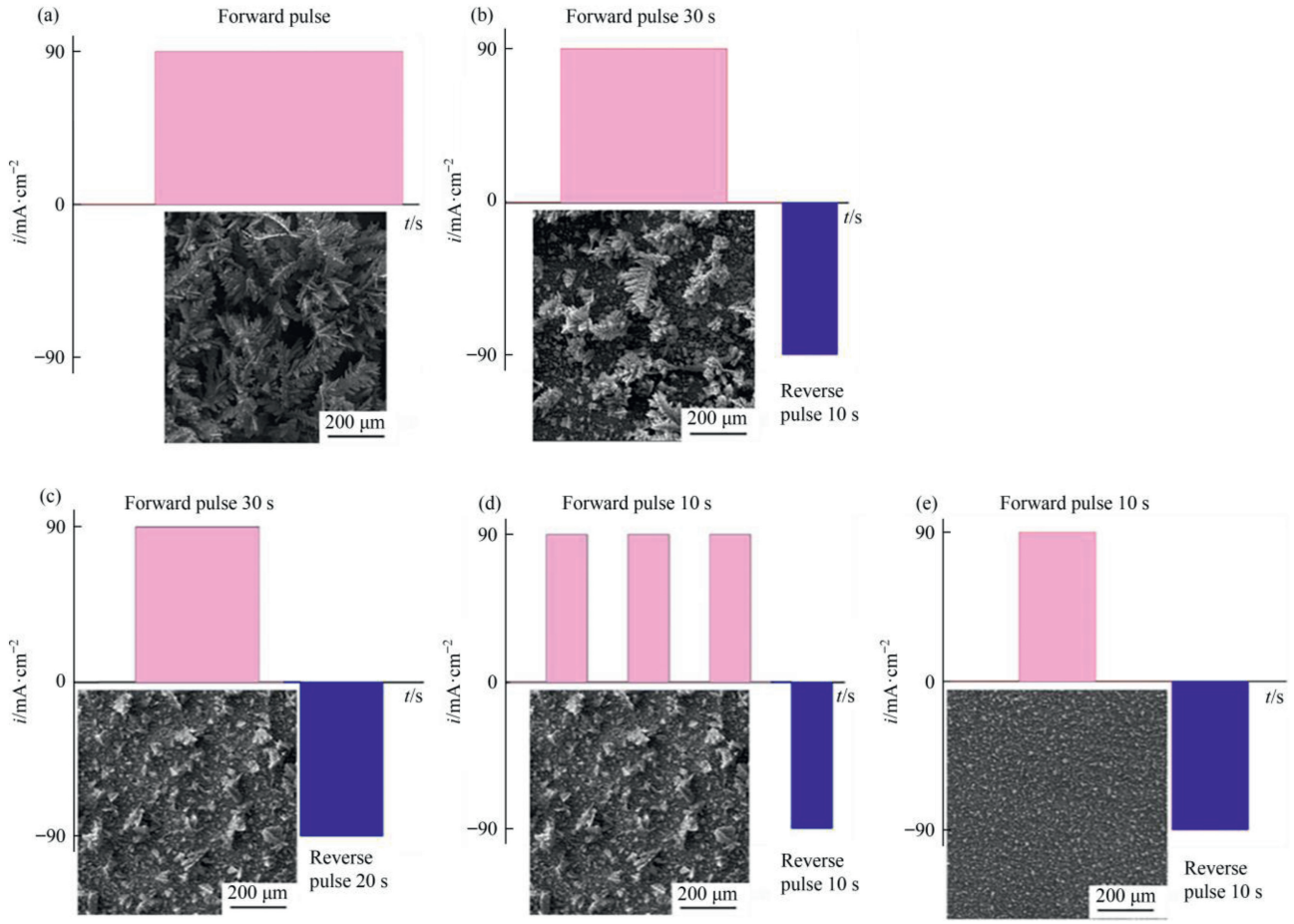

Fig. 15. Influences of different pulse charging methods on the growth of zinc dendrites: (a) forward constant current charge, (b) forward continuous pulse 30 s, reverse pulse 10 s, 5 s in the middle, (c) forward continuous pulse 30 s, reverse pulse 20 s, 5 s in the middle, (d) forward intermittent pulse 30 s, reverse pulse 10 s, 5 s in the middle, (e) forward pulse is 10 s, reverse pulse 10 s, middle 5 s.

electrolyte and changes the direction of the concentration gradient of the Zn ions at the tip of Zn dendrites, resulting in a change in the growth direction of the Zn dendrites increasing the flow rate of the electrolyte can effectively prolong the time for Zn dendrites to reach the other electrode and reduce the risk of short circuits in Zn-air batteries. In summary, the optimal electrolyte flow rate for inhibiting the growth of Zn dendrites is 40 $ml \cdot min^{-1}$.

Zn-air batteries have been widely used; however, the growth of dendrites does lead to some hazards, such as dendritic growth can penetrate the diaphragm and cause an internal short circuit, even explosion [30]. Furthermore, the poor cycling performance and capacity fade, caused by the growth of dendritic and mossy Zn, has long hindered the application of Zn-air batteries [31]. Third, after the initial deposition, a relatively loose dendrite layer appears on the Zn metal surface, which causes the deposition of Zn ions over the dendrites to reduce the ion concentration in the surrounding electrolyte. Meanwhile, the local ion concentration is increased during the dissolution of Zn ions occurs at the roots of the dendrites. This process accelerates the formation of dead dendrites [31].

In this paper, a non-linear phase field model combined with the Butler-Volmer expression, which was developed to study dendrite growth during electrodeposition. Extensive simulations and experiments were conducted to explore techniques for reducing dendrites growth. The results indicate that the height of growth dendrites can be reduced effectively by changing the anisotropic strength, temperature, and charging method. The risk of puncturing the separator is reduced, the occurrence of battery short circuits is decreased, battery cycling stability is enhanced, and the service life of zinc air batteries is extended when the dendrites have transformed from towering to dwarf. By changing the anisotropic modulus, the number of lateral branches is efficaciously reduced, while the number of dead dendrites is also controlled availably.

5. Conclusions

In this study, a two-dimensional phase field model for dendrite growth in Zn-air batteries was established. The model can present the morphology and growth of Zn dendrites. The dendrite growth mechanism of a Zn-air battery was studied using this model, and different suppression strategies were designed to inhibit the growth of Zn dendrites based on simulations of the Zn dendrite growth mechanism. The study has some reference values for dendritic problems in metal electrodeposition. In summary, the following conclusions can be drawn.

(1) The dendrite growth model was validated by changing the charging time. We concluded that the number of dendrite growths and the height gradually increased with an extension of the charging time. Therefore, the Zn ion concentration

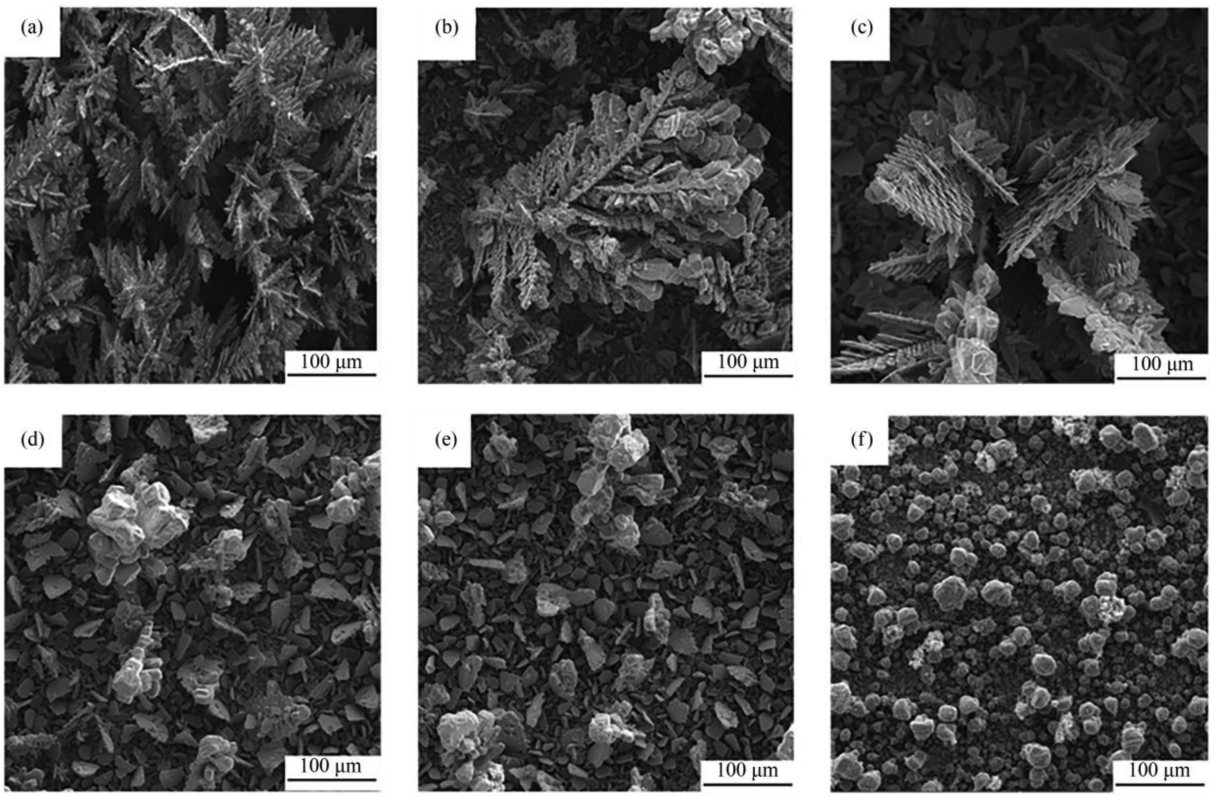

Fig. 16. Influence of electrolyte temperature on Zn dendrite growth, where represent the electrolyte temperature of 298.15 K (a), 303.15 K (b), 313.15 K (c), 323.15 K (d), 333.15 K (e), and 343.15 K (f), respectively.

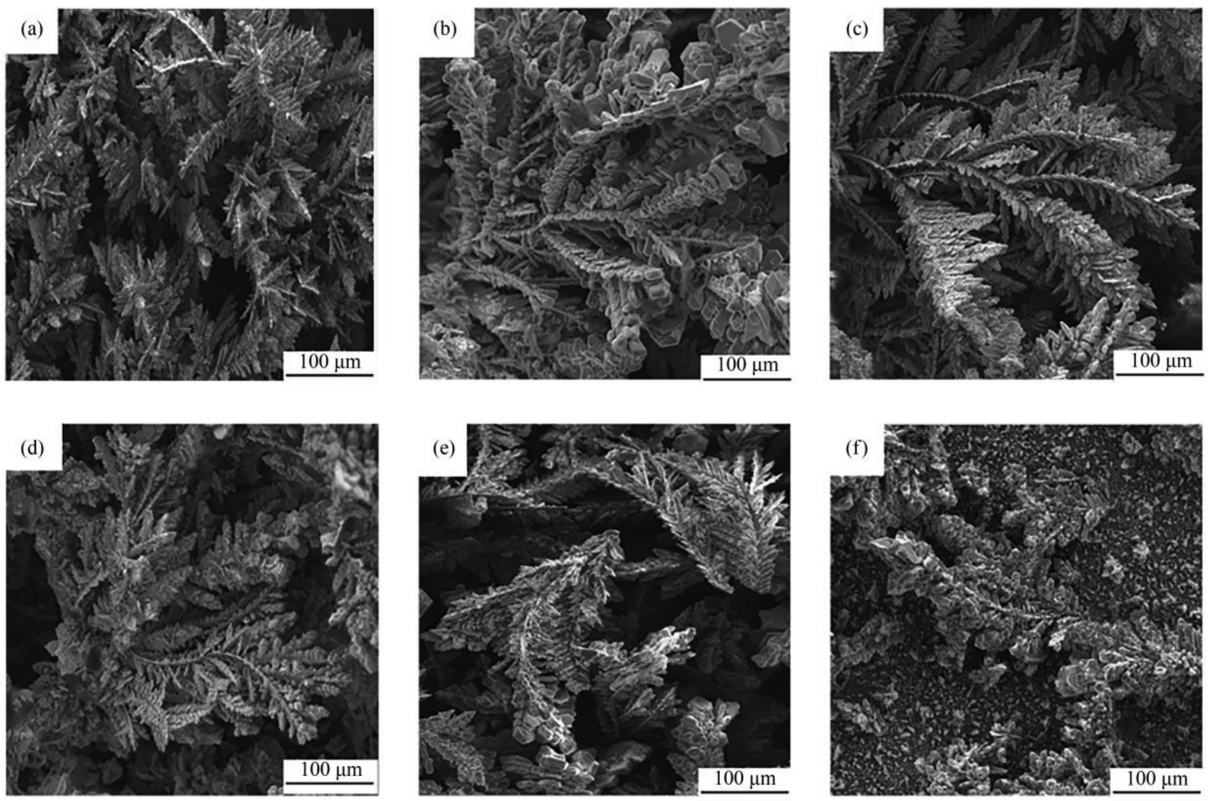

Fig. 17. Influence of electrolyte flow rate on Zn dendrite growth: (a) static electrolyte, (b) flow rate of electrolyte of 10 ml·min^{-1}, (c) flow rate of electrolyte of 20 ml·min^{-1}, (d) flow rate of electrolyte of 30 ml·min^{-1}, (e) flow rate of electrolyte of 35 ml·min^{-1}, (f) flow rate of electrolyte of 40 ml·min^{-1}.

gradient and the electric potential gradient are the two main driving forces for Zn dendrite growth. The experimental study further investigated the growth pattern of dendrites by changing the charging time under constant current charging. We concluded that the longer the constant current charging time is, the higher the growth height of Zn dendrites, consistent with the results of the simulations. Thus, the proposed model is reliable.

(2) The simulations show that the longer the charging time is, the higher the number of Zn dendrite growths, and the higher the growth height. The higher the intensity of the interfacial anisotropy is, the higher the number of nucleation sites of Zn dendrites and the higher the height of the Zn dendrite growth. The lower the temperature of the electrolyte is, the higher the dendrite growth height, mainly because the lower the temperature is, the more prejudiced diffusion and mass transfer processes of the Zn ions in the electrolyte, leading to an increasing concentration gradient of Zn ions at the tip of the dendrites, and Zn ions are preferentially deposited at the tip of the dendrites. Therefore, it is beneficial to restrain the growth of Zn dendrites by adopting measures to strengthen the ion diffusion and mass transfer in the electrolyte. The optimal electrolyte temperature is 343.15 K, and the inhibition of Zn dendrites reaches up to 59%. The uneven distribution of the electric potential is another main factor promoting the growth of Zn dendrites. The uneven distribution of the electric potential causes the local current density at the tip of the dendrite to be excessively high, prompting additional Zn ions to move from the tip of the dendrite and deposit. Therefore, reducing the potential gradient is effective in inhibiting dendrite growth in Zn-air batteries.

(3) The experiments show that the Zn alloy anode changes the interfacial anisotropy modulus. The larger the interfacial energy anisotropy modulus is, the more favorable the reduction in the height of Zn dendrite growth and the change in its growth direction. The best inhibition of dendrite growth in Zn-air batteries is the composition of 96.5% Zn-3.5% In or 93.5% Zn-6.5% Yb. The different pulses inhibit the growth of Zn dendrites by improving the uneven distribution of local current density at the tips of dendrites. The pulses of standing for 5 s, a forward pulse for 10 s, standing for 5 s, and a reverse pulse for 10 s are the best way to inhibit dendritic growth in the Zn-air battery. Increasing the electrolyte temperature and electrolyte flow rate enhances the diffusion and mass transfer process of Zn ions, further improving the ion concentration gradient at the tip of Zn dendrites. We concluded that the optimal electrolyte temperature is 343.15 K and the optimal electrolyte flow rate was 40 $mL \cdot min^{-1}$.

Declaration of Interest

The authors declare that they have no known competing financial interests or personal relationships that could have appeared to influence the work reported in this paper.

Acknowledgements

This work was financially supported by the National Natural Science Foundation of China (22168019 and 52074141) and the Major Science and Technology Projects in Yunnan Province (202202AB080014). The authors are grateful to the National Natural Science Foundation of China and the Major Science and Technology Projects in Yunnan Province for their support.

References

[1] X. Zhang, L.X. Zhu, X.C. Wang, S.P. Li, H.F. Wang, Latest research progress in Zn anode of secondary Zn-air batteries, *Chin. J. Nonferrous Metals* 30 (8) (2020) 1895–1905. (in Chinese)
[2] Zhao Lu, Electrochemical reaction model of zinc-air battery and research on dendrite growth inhibition, Master Thesis, Kunming University of Science and Technology, China, 2021. (in Chinese)
[3] Y.J. Zheng, N. Yang, J. Li, Y.Q. Hou, G. Xie, Research status of dendrite growth simulation of Zn-air battery, *Yunnan Metall.* 49 (3) (2020) 37–43. (in Chinese)
[4] A. Poosapati, K. Negrete, M. Thorpe, J. Hutchison, M. Zupan, Y.C. Lan, D. Madan, Safe and flexible chitosan-based polymer gel as an electrolyte for use in zinc-alkaline based chemistries, *J. Appl. Polym. Sci.* 138 (33) (2021) 138.
[5] D.F. Du, S. Zhao, Z. Zhu, F.J. Li, J. Chen, Photo-excited oxygen reduction and oxygen evolution reactions enable a high-performance Zn–air battery, *Angew. Chem.* 132 (41) (2020) 18297–18301.
[6] R.G. Gunther, R.M. Bendert, Zinc electrode shape change in cells with controlled current distribution, *J. Electrochem. Soc.* 134 (4) (1987) 782–791.
[7] J. McBreen, Zinc electrode shape change in secondary cells, *J. Electrochem. Soc.* 119 (12) (1972) 1620.
[8] C. Yang, Z.J. Zhan, Z.L. Tian, Y.Q. Lai, K. Zhang, J. Li, Effects of various carboxymethyl celluloses on the electrochemical characteristics of zinc anode from an alkaline electrolyte, *Electrochim. Acta* 163 (9) (2017) 284–290.
[9] L.N. Bengoa, S. Bruno, H.A. Lazzarino, P.R. Seré, W.A. Egli, Study of dendritic growth of zinc crystals on the edges of steel sheet, *J. Appl. Electrochem.* 44 (12) (2014) 1261–1269.
[10] S.J. Banik, R. Akolkar, Suppressing dendrite growth during zinc electrodeposition by PEG-200 additive, *J. Electrochem. Soc.* 160 (11) (2013) D519–D523.
[11] S.J. Banik, R. Akolkar, Suppressing dendritic growth during alkaline zinc electrodeposition using polyethylenimine additive, *Electrochim. Acta* 179 (2015) 475–481.
[12] J.M. Wang, L. Zhang, C. Zhang, X. Xiao, Q.Q. Zhang, C.N. Cao, The influence of Bi3+ and tetrabutylammonium bromide on the dendritic growth behavior of alkaline rechargeable Zn electrode, *J. Funct. Mater.* 32 (1) (2001) 45–47.
[13] S.J. Banik, R. Akolkar, Suppressing dendrite growth during zinc electrodeposition by PEG-200 additive, *J. Electrochem. Soc.* 160 (11) (2013) D519–D523.
[14] K.L. Wang, P.C. Pei, Z. Ma, H.C. Xu, P.C. Li, X.Z. Wang, Morphology control of zinc regeneration for zinc–air fuel cell and battery, *J. Power Sources* 271 (2014) 65–75.
[15] K.L. Wang, P.C. Pei, Y.C. Wang, Magnetic field improving interfacial behavior of the two-electrode system, *J. Electrochem. Soc.* 164 (13) (2017) A3440–A3444.
[16] Y.D. Liu, Q. Liu, L. Xin, Y.Z. Liu, F. Yang, E.A. Stach, J.A. Xie, Making Li-metal electrodes rechargeable by controlling the dendrite growth direction, *Nat. Energy* 2 (7) (2017) 17083.
[17] M. Shapouri Ghazvini, G. Pulletikurthi, Z. Liu, A. Prowald, S. Zein El Abedin, F. Endres, Electrodeposition and stripping behavior of a zinc/polystyrene composite electrode in an ionic liquid, *J. Solid State Electrochem.* 19 (5) (2015) 1453–1461.
[18] K.L. Wang, P.C. Pei, Z. Ma, H.C. Chen, H.C. Xu, D.F. Chen, X.Z. Wang, Dendrite growth in the recharging process of zinc–air batteries, *J. Mater. Chem. A* 3 (45) (2015) 22648–22655.
[19] E.R. White, S.B. Singer, V. Augustyn, W.A. Hubbard, M. Mecklenburg, B. Dunn, B.C. Regan, *In situ* transmission electron microscopy of lead dendrites and lead ions in aqueous solution, *ACS Nano* 6 (7) (2012) 6308–6317.
[20] J.S. Keist, C.A. Orme, P.K. Wright, J.W. Evans, An *in situ* AFM study of the evolution of surface roughness for zinc electrodeposition within an imidazolium based ionic liquid electrolyte, *Electrochim. Acta* 152 (2015) 161–171.
[21] L.A. Guo, A. Radisic, P.C. Searson, Kinetic Monte Carlo simulations of nucleation and growth in electrodeposition, *J. Phys. Chem. B* 109 (50) (2005) 24008–24015.
[22] L.Y. Liang, Y.E. Qi, F. Xue, S. Bhattacharya, S.J. Harris, L.Q. Chen, Nonlinear phase-field model for electrode-electrolyte interface evolution, *Phys. Rev. E* 86 (5) (2012) 051609.
[23] L. Chen, H.W. Zhang, L.Y. Liang, Z. Liu, Y.E. Qi, P. Lu, J. Chen, L.Q. Chen, Modulation of dendritic patterns during electrodeposition: A nonlinear phase-field model, *J. Power Sources* 300 (2015) 376–385.
[24] K.L. Wang, X.T. Liu, P.C. Pei, Y. Xiao, Y.C. Wang, Guiding bubble motion of rechargeable zinc-air battery with electromagnetic force, *Chem. Eng. J.* 352 (2018) 182–187.
[25] K.L. Wang, P.C. Pei, Y.C. Wang, C. Liao, W. Wang, S.W. Huang, Advanced rechargeable zinc-air battery with parameter optimization, *Appl. Energy* 225 (2018) 848–856.
[26] P. Li, H.L. Wang, X.H. Tan, W. Hu, M.H. Huang, J. Shi, J.W. Chen, S. Liu, Z.C. Shi, Z. Li, Bifunctional electrocatalyst with CoN_3 active sties dispersed on N-doped

graphitic carbon nanosheets for ultrastable Zn-air batteries, *Appl. Catal. B* 316 (2022) 121674.
[27] X.J. Zheng, X.C. Cao, Y. Zhang, K. Zeng, L. Chen, R.Z. Yang, Tunable dual cationic redox couples boost bifunctional oxygen electrocatalysis for long-term rechargeable Zn-air batteries, *J. Colloid Interface Sci.* 628 (2022) 922–930.
[28] H.W. Chen, Y.J. Liu, B. Liu, M. Yang, H.M. Li, H.B. Chen, Hypercrosslinked polymer-mediated fabrication of binary metal phosphide decorated spherical carbon as an efficient and durable bifunctional electrocatalyst for rechargeable Zn–air batteries, *Nanoscale* 14 (34) (2022) 12431–12436.
[29] Y.N. Jo, P. Santhoshkumar, K. Prasanna, K. Vediappan, C.W. Lee, Improving self-discharge and anti-corrosion performance of Zn-air batteries using conductive polymer-coated Zn active materials, *J. Ind. Eng. Chem.* 76 (2019) 396–402.
[30] H. Jing, H. Xing, X.L. Dong, Y.S. Han, Nonlinear phase-field modeling of lithium dendritic growth during electrodeposition, *J. Electrochem. Soc.* 169 (3) (2022) 032511.
[31] Y.T. He, F. Ding, L. Lin, Z.H. Wang, Z. Lü, Y.H. Zhang, Influence of interfacial concentration polarization on lithium metal electrodeposition, *Acta Phys. Chim. Sin.* 37 (2) (2020) 2009001.